Imaging Science in Dentistry 2021; 51: 413-9
https://doi.org/10.5624/isd.20210099

# Influence of receiver bandwidth on MRI artifacts caused by orthodontic brackets composed of different alloys

Reinaldo Abdala-Junior[1,3], Juliana No-Cortes[2], Emiko Saito Arita[1], Jerome L. Ackerman[3], Renan Lúcio Berbel da Silva[1,*], Jun Ho Kim[1,4], Arthur Rodriguez Gonzalez Cortes[1,3]

[1]*Department of Oral Radiology, School of Dentistry, University of São Paulo, São Paulo, SP, Brazil*
[2]*Department of Dental Surgery, Faculty of Dental Surgery, University of Malta, Msida, Malta*
[3]*Department of Radiology, Martinos Center of Biomedical Imaging, Massachusetts General Hospital, Charlestown, MA, USA*
[4]*Department of Oral and Maxillofacial Radiology, School of Dentistry, Seoul National University, Seoul, Korea*

## ABSTRACT

**Purpose**: The aim of this *in vitro* study was to assess the role of bandwidth on the area of magnetic resonance imaging (MRI) artifacts caused by orthodontic appliances composed of different alloys, using different pulse sequences in 1.5 T and 3.0 T magnetic fields.

**Materials and Methods**: Different phantoms containing orthodontic brackets (ceramic, ceramic bracket with a stainless-steel slot, and stainless steel) were immersed in agar gel and imaged in 1.5 T and 3.0 T MRI scanners. Pairs of gradient-echo (GE), spin-echo (SE), and ultrashort echo time (UTE) pulse sequences were used differing in bandwidth only. The area of artifacts from orthodontic devices was automatically estimated from pixel value thresholds within a region of interest (ROI). Mean values for similar pulse sequences differing in bandwidth were compared at 1.5 T and 3.0 T using analysis of variance.

**Results**: The comparison of groups revealed a significant inverse association between bandwidth values and artifact areas of the stainless-steel bracket and the self-ligating ceramic bracket with a stainless-steel slot ($P<0.05$). The areas of artifacts from the ceramic bracket were the smallest, but were not reduced significantly in pulse sequences with higher bandwidth values ($P<0.05$). Significant differences were also observed between 1.5 T and 3.0 T MRI using SE and UTE, but not using GE 2-dimensional or 3-dimensional pulse sequences.

**Conclusion**: Higher receiver bandwidth might be indicated to prevent artifacts from orthodontic appliances in 1.5 T and 3.0 T MRI using SE and UTE pulse sequences. ***(Imaging Sci Dent 2021; 51: 413-9)***

**KEY WORDS**: Dental Materials; Magnetic Resonance Imaging; Artifacts; Orthodontic Brackets

## Introduction

Magnetic resonance imaging (MRI) provides multiplanar imaging that is useful for oral diagnoses because of its features such as adequate soft-tissue contrast.[1-3] Although the method does not involve ionizing radiation, MRI is prone to artifacts caused by the presence of metallic devices[4] such as orthodontic brackets and arch wires. These are known as susceptibility artifacts, which arise from the magnetic properties of these materials, especially those made of stainless steel.[5]

Electrical currents from stainless steel brackets and wires generate their own local magnetic fields, which, when added to the fields intentionally imposed by the scanner, yield distorted net main, radiofrequency (RF), and gradient fields that in turn create image artifacts.[5] Even when MRI scanners are used within the RF and gradient field safety limitations, the inherent static magnetism of

This research was carried out at the Athinoula A. Martinos Center for Biomedical Imaging at the Massachusetts General Hospital, using resources provided by the Center for Functional Neuroimaging Technologies, P41EB015896, a P41 Biotechnology Resource Grant supported by the National Institute of Biomedical Imaging and Bioengineering (NIBIB), National Institutes of Health.
Received April 23, 2021; Revised May 13, 2021; Accepted May 14, 2021
Published online Aug 11, 2021
*Correspondence to : Dr. Renan Lúcio Berbel da Silva
Department of Stomatology, School of Dentistry, University of São Paulo, Avenida Professor Lineu Prestes, 2227. São Paulo, SP 05508-000, Brazil
Tel) 55-11-99404-3031, E-mail) renan.lucio.silva@usp.br

metallic orthodontic materials causes distortions in the main magnetic field generated by the scanner, creating susceptibility artifacts that may compromise the images or lead to an erroneous diagnosis.[6,7]

There are several ways of attempting to minimize the size of susceptibility artifacts. One of them is choosing optimized imaging protocols of pulse sequence type and parameters, as well as magnetic field strength.[5,7,8] In our previous study on 1.5 and 3.0 T MRI of metal-ceramic restorations, echo time (TE) and receiver bandwidth were found to affect the size of susceptibility artifacts significantly.[9] Nevertheless, little is known about the influence of receiver bandwidth on the extent of artifacts caused by orthodontic appliances.

Thus, the aim of this phantom study was to clarify how changes in receiver bandwidth affect susceptibility artifacts caused by orthodontic appliances composed of different alloys at 1.5 T and 3.0 T field strengths.

## Materials and Methods

### Samples

Three different types of orthodontic brackets (a ceramic bracket [Clarity Advanced, 3M Unitek, Monrovia, CA, USA]; a self-ligating ceramic bracket with a stainless-steel slot [Clarity SL, 3M Unitek, Monrovia, CA, USA]; and a stainless-steel metallic bracket) were assessed. Measurements of the ceramic bracket were considered control values in the study, since ceramic materials do not yield significant artifacts on MRI due to their very low magnetic susceptibility.[10]

### Phantom

The phantom of this study was constructed using a rectangular plastic Tupperware-style container measuring 128 × 128 × 40 mm. Half of the container volume was initially filled with a layer of hot 1% agar in water. A plastic wrap was used to cover the phantom to allow the gel to form at room temperature for 30 minutes. Each sample was then placed over the solid first layer of the agar gel, ensuring that the same MRI slice could be used to assess all objects (Fig. 1A). Next, the rest of the container was filled with a second layer of agar gel. As a result, all samples could be arrayed in the phantom's horizontal midplane. The 3 different types of brackets were evaluated at the same time in the same phantom. All MRI scans were acquired with the phantom within the container.

### MRI scans

A head coil was used in 2 different MRI scanners (1.5 T Avanto and 3.0 T Tim Trio, Siemens Medical Solutions, Erlangen, Germany) to scan phantoms along the coronal plane with a field of view of 180 mm × 180 mm × 180 mm and a matrix of 256 × 256 pixels. The RF pulse was set with a phase resolution of 100% in the "fast" mode. Pulse sequences differing in receiver bandwidth were adjusted to have all other parameters similar in both the 1.5 T and 3.0 T scans. The metadata windows of Digital Imaging and Communications in Medicine (DICOM) files were used to retrieve data regarding the flip angle, number of slices, and slice thickness in an open-source DICOM viewer (OsiriX v10.09.0, Pixmeo, Geneva, Switzerland), and this information was recorded. Images were obtained at 1.5 T and 3.0 T using gradient-echo (GE; 2-dimensional [2D] and 3-dimensional [3D]), spin-echo (SE), and ultrashort echo time (UTE) pulse sequences. Only 1 parameter varied in each comparison, while all other parameters were fixed. For instance, the exact same pulse sequences, with a bandwidth of 260

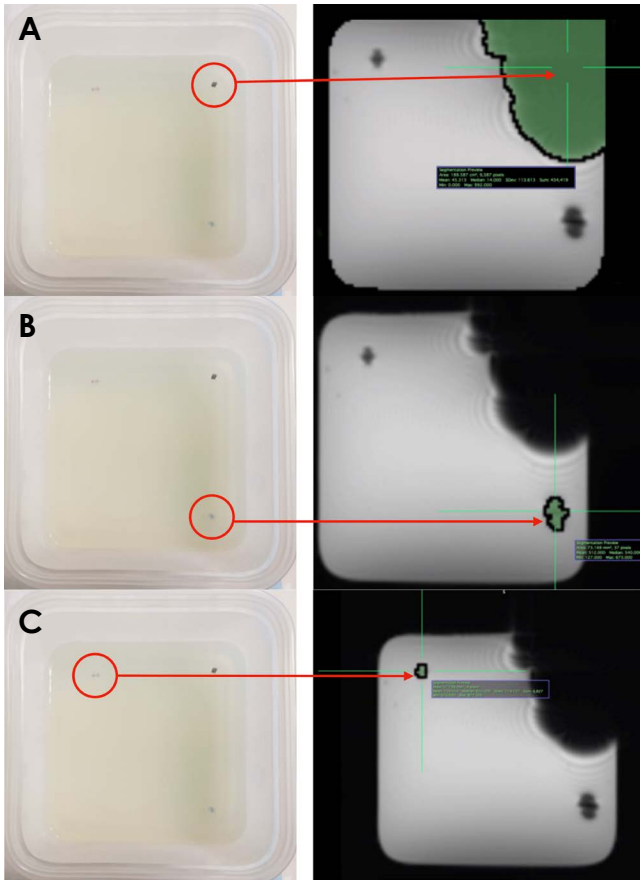


**Fig. 1.** Phantom used in the study with brackets and corresponding 3.0 T magnetic resonance images showing the threshold region-growing method used to perform automated measurements of the total area affected by the artifact. A. Ceramic bracket. B. Self-ligating bracket. C. Stainless steel bracket.

**Table 1.** Assessment of individual pulse sequence parameters used in MRI scans

| Field strength | Bandwidth | Type | TR | TE | ST | NS | NEX | FA |
|---|---|---|---|---|---|---|---|---|
| 1.5 T | 260 Hz; 780 Hz | GE | 200; 275 | 3.61; 5; 10; 20; 40 | 3 | 10 | 1 | 25 |
| | 260 Hz; 780 Hz | SE | 275 | 10; 20; 40 | 3 | 10 | 1 | 70 |
| | 260 Hz; 780 Hz; 1680 Hz | UTE | 13 | 0.07 | 1 | 192 | 1 | 10 |
| 3.0 T | 260 Hz; 780 Hz | GE | 275; 600 | 3.61; 5; 10; 20; 40; 80 | 3 | 10 | 1; 4 | 50; 30 |
| | 260 Hz; 780 Hz | SE | 275; 600 | 5; 10; 20; 40; 80 | 3 | 10 | 1; 4 | 115 |
| | 260 Hz; 780 Hz; 1680 Hz | UTE | 3.16, 600 | 0.07 | 1 | 192 | 1 | 10; 15 |

GE: gradient echo, SE: spin echo, UTE: ultrashort echo time, TR: repetition time, TE: echo time, ST: slice thickness, NS: number of slices, NEX: number of experiments (average), FA: flip angle

Hz, were also tested with a bandwidth of 780 Hz, and so forth. All pulse sequence parameters used in this study are shown in Table 1.

### Artifact measurement

The areas occupied by artifacts were measured from pixel values using the threshold tool of a free imaging software (ImageJ® v1.53a, National Institutes of Health, Bethesda, MD, USA). A region of interest (ROI) enclosing the area with signal loss caused by the 3 types of brackets and the respective artifacts was generated, following a previously described methodology.[11] All artifact areas were measured in the mid-slice containing each orthodontic device. The threshold considered was defined according to the signal intensity histogram (grayscale values ranging from 0 to 255). Mean, minimum, and maximum pixel values were recorded. The range of threshold values was optimized to a minimum of 0 and a maximum of 180 for all measurements. Therefore, all pixels in the aforementioned range were classified as artifacts and included in the auto-generated ROI. An area measurement tool in the same imaging software was then used to calculate the ROI area in millimeters squared (Fig. 1). Because this is an entirely automated and reproducible method, a single observer performed all measurements.

### Statistical analysis

The sample size ($n$ = number of artifact images for each sample) calculation was carried out considering a statistical power of 80%, at a level of significance of 5%, with the uncorrected chi-square test. The normality of artifact area measurements was evaluated using the Shapiro-Wilk test ($P > 0.05$).

Statistical comparisons between mean artifact areas using low and high receiver bandwidth, different pulse sequences, and different field strengths were assessed using analysis of variance (ANOVA). Bracket type was also evaluated using ANOVA. Individual differences were assessed with the *post hoc* Tukey test. This set of experimental variations was done to evaluate the sole influence of receiver bandwidth and each other factor analyzed on the artifact size. All statistical analyses were performed using SPSS version 17.0 (SPSS Inc., Chicago, IL, USA). A $P$-value under 0.05 was considered to indicate statistical significance.

**Table 2.** Comparisons of mean artifact area measurements using the same pulse sequences for each type of bracket, MRI field strength, receiver bandwidth and pulse sequence type

| Varying parameter | Area ($mm^2$) |
|---|---|
| Receiver bandwidth* | |
| 260 Hz | 804.3 ± 1170.6 |
| 780 Hz | 768.7 ± 1169.1 |
| 1680 Hz | 359.7 ± 543.0 |
| Pulse sequence type* | |
| D | 993.5 ± 1409.8 |
| GE 3D | 1009.6 ± 1430.3 |
| SE | 489.0 ± 757.9 |
| UTE | 555.8 ± 830.2 |
| MRI field strength* | |
| 1.5 T | 656.2 ± 1025.3 |
| 3.0 T | 822.0 ± 1204.3 |
| Bracket* | |
| Ceramic | 15.6 ± 5.0 |
| Self-ligating | 46.5 ± 28.1 |
| Stainless steel | 2155.1 ± 813.6 |

*$P < 0.05$ using analysis of variance, GE: gradient echo, SE: spin echo, UTE: ultrashort echo time

## Results

A total of 54 MRI artifact images (27 from the 1.5 T field

**Table 3.** Individual comparisons from analysis of variance results, obtained using the *post hoc* Tukey test

| Bracket | Comparisons | Multiple differences and 95% confidence intervals | | |
|---|---|---|---|---|
| | | Estimated | Lower | Higher |
| Ceramic | Receiver bandwidth | | | |
| | 260 Hz × 780 Hz | −0.87 | −4.80 | 3.07 |
| | 260 Hz × 1680 Hz | −3.53 | −9.75 | 2.70 |
| | 780 Hz × 1680 Hz | −2.66 | −8.88 | 3.57 |
| | Pulse sequence type | | | |
| | GE 3D × GE 2D* | 6.43 | 0.23 | 12.63 |
| | SE × GE-2D | 0.20 | −6.20 | 6.20 |
| | UTE × GE-2D | −3.91 | −9.58 | 1.75 |
| | SE × GE-3D* | −6.43 | −12.63 | −0.23 |
| | UTE × GE-3D* | −10.34 | −16.01 | −4.68 |
| | UTE × SE | −3.91 | −9.57 | 1.75 |
| | MRI field strength | | | |
| | 3.0 T × 1.5 T | 0.44 | −2.58 | 3.47 |
| Self-ligating | Receiver bandwidth | | | |
| | 260 Hz × 780 Hz | −9.40 | −26.23 | 7.43 |
| | 260 Hz × 1680 Hz* | −42.59 | −69.20 | −15.98 |
| | 780 Hz × 1680 Hz* | −33.19 | −59.81 | −6.58 |
| | Pulse sequence type | | | |
| | GE-3D × GE-2D | −5.44 | −31.96 | 21.09 |
| | SE × GE-2D* | −47.71 | −74.23 | −21.18 |
| | UTE × GE-2D* | −30.38 | −54.60 | −6.17 |
| | SE × GE-3D* | −42.27 | −68.79 | −15.75 |
| | UTE × GE-3D* | −24.95 | −49.16 | −0.73 |
| | UTE × SE | 17.32 | −6.89 | 41.54 |
| | MRI field strength | | | |
| | 3.0 T × 1.5 T* | 23.40 | 10.47 | 36.33 |
| Stainless-steel | Receiver bandwidth | | | |
| | 260 Hz × 780 Hz | −96.63 | −458.44 | 265.19 |
| | 260 Hz × 1680 Hz* | −1287.63 | −1859.71 | −715.54 |
| | 780 Hz × 1680 Hz* | −1191 | −1763.09 | −618.91 |
| | Pulse sequence type | | | |
| | GE-3D × GE-2D | 47.25 | −522.92 | 617.42 |
| | SE × GE-2D* | −1465.75 | −2035.92 | −895.58 |
| | UTE × GE-2D* | −851.90 | −1372.39 | −331.40 |
| | SE × GE-3D* | −1513 | −2083.17 | −942.83 |
| | UTE × GE-3D* | −899.15 | −1419.64 | −378.65 |
| | UTE × SE* | 613.85 | 93.36 | 1134.35 |
| | MRI field strength | | | |
| | 3.0 T × 1.5 T* | 473.56 | 195.56 | 751.55 |

*: $P<0.05$, GE: gradient echo, SE: spin echo, UTE: ultrashort echo time

and 27 from the 3.0 T field) were analyzed. A normal distribution was confirmed for all measurements according to the Shapiro-Wilk test ($P>0.05$). A comparison of the mean artifact area with ANOVA revealed significant differences among types of brackets, pulse sequences, field strengths, and receiver bandwidths ($P<0.05$, Table 2 and Fig. 2). The

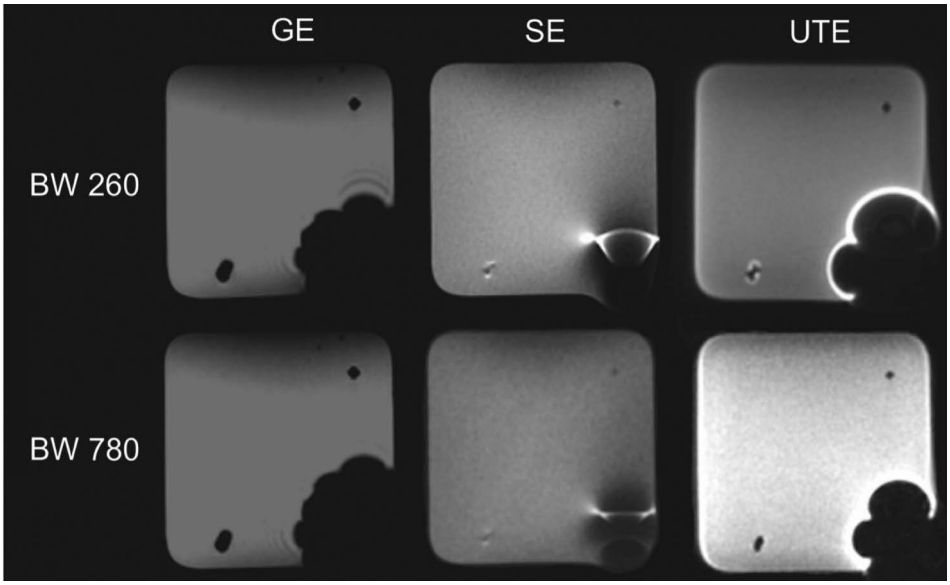


**Fig. 2.** Comparison among GE, SE and UTE pulse sequences on 1.5 T MRI varying in receiver bandwidth (BW). Note that the SE and UTE images are affected by differences in the receiver bandwidth.

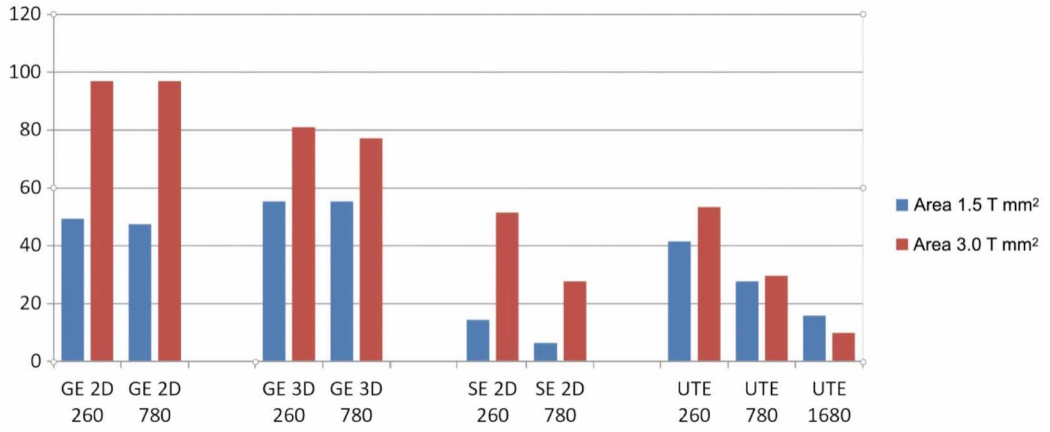


**Fig. 3.** Bar graph shows the mean artifact area measurements considering all magnetic resonance imaging pulse sequences with only the receiver bandwidth values varying (i.e., 260, 780, and 1680 Hz).

mean artifact areas of each type of orthodontic bracket analyzed using GE, SE, and UTE at 1.5 T and 3.0 T are available in Tables 2 and 3.

The results of the individual statistical comparisons using the Tukey test are available in Table 3. Higher receiver bandwidth values in both 1.5 T and 3.0 T MRI significantly reduced artifacts for the stainless-steel bracket with SE and UTE pulse sequences ($P<0.05$), and for the self-ligating bracket with UTE pulse sequences ($P<0.05$, but not for the ceramic bracket ($P>0.05$), which presented the lowest artifact areas of the study. However, in the GE 2D and 3D images, a higher receiver bandwidth did not lead to significant reductions in the artifact area ($P>0.05$, respectively; Fig. 3).

## Discussion

Procedures to remove orthodontic bonded appliances, such as metallic brackets, are considered time-consuming and uncomfortable for the patient, and pose a risk of damaging the enamel. Researchers have reported that ceramic brackets and appliances had low magnetic susceptibility.[8,10] Significant MRI artifacts can be generated by electrical currents caused by stainless steel orthodontic appliances, which are commonly used.[10,11] In addition, these electrical currents cause heating of the material and the surrounding tissue, and therefore constitute a safety concern requiring faster scans using optimized MRI protocols to minimize artifacts as much as possible.

To minimize the metallic artifacts near a metallic prosthesis, advanced MRI techniques such as slice encoding for metal artifact correction (SEMAC) and multiacquisition variable resonance image combination (MAVRIC) have been suggested. The SEMAC sequence is a metal-artifact reduction MRI technique based on 2D view angle tilting (VAT) and can provide robust encoding of excited slices against metal-induced field inhomogeneities within a feasible scan time. By combining the data resolved from multiple SEMAC-corrected slices and using VAT, SEMAC can be used to correct for spatial distortions.[11] Many challenges have been associated with 3.0 T MRI of the spine, such as how to handle increases in the signal-to-noise ratio (SNR), how to optimize diagnostic quality, and how to improve the clinical impact.

Previous medical studies of different metallic devices have described an inverse relationship between receiver bandwidth and the extent of MRI susceptibility artifacts.[12,13] These findings corroborate the present results for SE and UTE, but not for GE pulse sequences. In addition, the present study addressed the use of receiver bandwidth values of 1680 with UTE pulse sequences, which led to smaller artifact areas at 3.0 T, even in comparison with 1.5 T. However, a higher receiver bandwidth led to a lower SNR, which is a direct measurement of image quality.

In contrast with our results, a previous study[14] concluded that increasing receiver bandwidth did not show any influence on artifacts when the matrix was larger than 256 × 256. Increasing matrix size was also considered as a way of decreasing artifact area extensions. However, SNR loss should be avoided, because it has been suggested that increasing bandwidth is a better method than increasing the matrix to minimize artifacts without compromising the SNR and MRI image quality.[15]

According to the statistical differences found between artifacts from 1.5 T and 3.0 T, SE pulse sequences with the higher option of bandwidth values used herein led to artifact reductions of up to 35%. However, the same finding was not observed for GE 3D pulse sequences. The aforementioned findings support those of a similar study on medical metallic devices.[12] Increasing bandwidth values enable the application of a larger magnetic field gradient in the scanner while the MR signal is digitized during the frequency encoding step. This reduction of the artifact frequency may have shifted the relative bandwidth per pixel, causing the artifact to occur in a smaller number of pixels.[15] According to the findings of the present study, UTE pulse sequences allowed smaller artifact areas than the SE and GE pulse sequence protocols. These results are in accordance with our previous study on artifacts from metal-ceramic prostheses.[9] Reichert et al.[16] reported that UTE pulse sequences are the most indicated for visualizing solid structures, and several authors[2,17] have described UTE as useful for differentiating tissues in oral diagnoses. The main reasons attributed for those advantages of UTE are the use of very short echo times and high bandwidth values, keeping satisfactory contrast resolution while resulting in relatively small artifact areas in both 1.5 and 3.0 T magnetic fields.[9] Nevertheless, a limitation of the present study is the restricted range of editable parameters in the pre-commercial UTE pulse sequence provided by the manufacturer of the scanner of this study, preventing any further statistical comparisons.

In conclusion, ceramic brackets were the least affected by changes in MRI parameters. In addition, higher receiver bandwidth can be recommended to minimize artifacts caused by orthodontic appliances in scans from 1.5 T and 3.0 T MRI using SE and UTE, but not GE pulse sequences.

**Conflicts of Interest:** None

## References

1. Aguiar MF, Marques AP, Carvalho AC, Cavalcanti MG. Accuracy of magnetic resonance imaging compared with computed tomography for implant planning. Clin Oral Implants Res 2008; 19: 362-5.
2. Bracher AK, Hofmann C, Bornstedt A, Hell E, Janke F, Ulrici J, et al. Ultrashort echo time (UTE) MRI for the assessment of caries lesions. Dentomaxillofac Radiol 2013; 42: 20120321.
3. Nagamatsu-Sakaguchi C, Maekawa K, Ono T, Yanagi Y, Minakuchi H, Miyawaki S, et al. Test-retest reliability of MRI-based disk position diagnosis of the temporomandibular joint. Clin Oral Investig 2012; 16: 101-8.
4. Senel FC, Duran S, Icten O, Izbudak I, Cizmeci F. Assessment of the sinus lift operation by magnetic resonance imaging. Br J Oral Maxillofac Surg 2006; 44: 511-4.
5. Schenck JF. The role of magnetic susceptibility in magnetic resonance imaging: MRI magnetic compatibility of the first and second kinds. Med Phys 1996; 23: 815-50.
6. Beuf O, Lissac M, Crémillieux Y, Briguet A. Correlation between magnetic resonance imaging disturbances and the magnetic susceptibility of dental materials. Dent Mater 1994; 10: 265-8.
7. Bui FM, Bott K, Mintchev MP. A quantitative study of the pixel-shifting, blurring and nonlinear distortions in MRI images caused by the presence of metal implants. J Med Eng Technol 2000; 24: 20-7.
8. Hubálková H, Hora K, Seidl Z, Krásenský J. Dental materials and magnetic resonance imaging. Eur J Prosthodont Restor

Dent 2002; 10: 125-30.
9. Cortes AR, Abdala-Junior R, Weber M, Arita ES, Ackerman JL. Influence of pulse sequence parameters at 1.5 T and 3.0 T on MRI artefacts produced by metal-ceramic restorations. Dentomaxillofac Radiol 2015; 44: 20150136.
10. Starcuková J, Starcuk Z Jr, Hubálková H, Linetskiy I. Magnetic susceptibility and electrical conductivity of metallic dental materials and their impact on MR imaging artifacts. Dent Mater 2008; 24: 715-23.
11. Klinke T, Daboul A, Maron J, Gredes T, Puls R, Jaghsi A, et al. Artifacts in magnetic resonance imaging and computed tomography caused by dental materials. PLoS One 2012; 7: e31766.
12. Olsrud J, Lätt J, Brockstedt S, Romner B, Björkman-Burtscher IM. Magnetic resonance imaging artifacts caused by aneurysm clips and shunt valves: dependence on field strength (1.5 and 3 T) and imaging parameters. J Magn Reson Imaging 2005; 22: 433-7.
13. Lüdeke KM, Röschmann P, Tischler R. Susceptibility artefacts in NMR imaging. Magn Reson Imaging 1985; 3: 329-43.
14. Toms AP, Smith-Bateman C, Malcolm PN, Cahir J, Graves M. Optimization of metal artefact reduction (MAR) sequences for MRI of total hip prostheses. Clin Radiol 2010; 65: 447-52.
15. Hilgenfeld T, Prager M, Heil A, Schwindling FS, Nittka M, Grodzki D, et al. PETRA, MSVAT-SPACE and SEMAC sequences for metal artefact reduction in dental MR imaging. Eur Radiol 2017; 27: 5104-12.
16. Reichert IL, Robson MD, Gatehouse PD, He T, Chappell KE, Holmes J, et al. Magnetic resonance imaging of cortical bone with ultrashort TE pulse sequences. Magn Reson Imaging 2005; 23: 611-8.
17. Hövener JB, Zwick S, Leupold J, Eisenbeiβ AK, Scheifele C, Schellenberger F, et al. Dental MRI: imaging of soft and solid components without ionizing radiation. J Magn Reson Imaging 2012; 36: 841-6.